PIV MEASUREMENTS IN IMPINGING JETS AT A HIGH REYNOLDS NUMBER

Leon F.G. Geers **Mark J. Tummers** **Kemal Hanjalić**
Department of Applied Physics
Delft University of Technology
PO Box 5046, 2600 GA Delft
The Netherlands
e-mail: leon@ws.tn.tudelft.nl

ABSTRACT

The focus of the paper is on detailed measurements of mean flow and turbulence in the impingement zone of a multiple impinging jet set-up, using Particle Image Velocimetry (PIV). In order to verify our PIV system, the results of PIV and LDA measurements were conducted in a single impinging jet. Good agreement was observed between the results of both techniques. Subsequently, PIV measurements provided mean and fluctuating velocity fields in three planes in a multiple impinging jet set-up. A horse shoe type vortex was observed that circumscribes the outer jet of the array. Furthermore, compared to a single impinging jet the potential core of the central jet is significantly shorter.

INTRODUCTION

Impinging jets are used frequently to achieve intensive heating or cooling in various technological applications. Heat transfer enhancement depends, however, on a number of parameters: nozzle shape and its distance from the wall, initial flow field and turbulence in the jet, the surrounding near-field boundary conditions etc. In case of multiple jets, the nozzle arrangement and mutual distance are additional parameters. Engineering-type correlation for integral Nusselt number in terms of Reynolds number and geometry or configuration parameters have been reported in the literature, see e.g. Viskanta (1993), Martin (1977). Some results are also available for the time-averaged distribution of heat transfer coefficients or temperature on the impinged plate. Strong effects of some of the parameters have been observed not only on the total heat transfer enhancement, but also on the uniformity of the temperature distribution, which is often a crucial prerequisite for the quality of the technological process. While the mean temperature distribution on the plate reflects on the whole the typical mean flow pattern, the presence of organized and coherent vortical structure may have a profound local influence (Kataoka, 1990). Even in the simple configuration of a round initially non-turbulent uniform jet issuing from a nozzle, a street of initially toroidal vortices, that eventually break down into coherent eddy structures, will influence the mixing in the jet. These structures will also penetrate the impinged wall boundary layer, affecting thus the heat transfer. These effects will depend primarily on the nozzle-wall distance, but also on other parameters. In a multi-jet configuration, interaction between the neighbouring jets can generate complex and unstable secondary motions and large eddy structures (e.g. Moustafa and Rathakrishnan, 1993), which may strongly affect the local temperature distribution. Various methods of heat transfer enhancement target directly or indirectly these large eddy structures. However, very little is known about the eddy morphology in multiple-jet configurations and physical mechanism by which they augment or suppress the local heat transfer. This paper aims at providing some information in that direction.

We report here on the ongoing research project aimed at investigating the flow and turbulence structure in a single and multiple impinging jets, and their correlation with the instantaneous wall temperature field. The final goal is to provide guidelines for optimization of cooling and heating process in various applications. While many issues are still to be addressed, we present here some results obtained in an isothermal situation in which multiple jets issuing from nozzles, impinge normally on a flat wall. The focus of the paper is on detailed measurements of mean flow and turbulence, as well as on detecting and identifying coherent structure in the impingement zone, using Par-

ticle Image Velocimetry (PIV).

EXPERIMENTAL METHOD

First a series of experiments was conducted in a single impinging jet using Particle Image Velocimetry (PIV). The jet was issued from a pipe with a diameter d of 36 mm and length L of 2.74 m, placed perpendicular to a flat plate at a distance of 72 mm ($2d$). The axial and radial velocity components were measured in a plane of $1.6d\times$ $1.6d$ at a Reynolds number of 23 $\times 10^3$. In order to verify the consistency of the PIV measurements, also Laser Doppler Anemometry (LDA) measurements were done in this geometry.

The LDA measurements were performed using a two-component, fibre optic, dual beam system. The green (514.5 μm) and blue (488.0 μm) colours of a 5 W Argon-ion laser were used to measure two components of the velocity simultaneously. One beam of each colour was frequency shifted 40 MHz by a Bragg cell to detect instantaneous flow reversals. The length and diameter of the two overlapping measurement volumes are 1.7 mm and 0.12 mm, respectively. The photomultiplier output signals were electronically down-mixed, and subsequently fed to two IFA-750 signal processors.

The PIV system (manufactured by Optical Flow Systems, OFS) included a Nd:YAG laser with a pulse energy of 25 mJ. This laser produced a 1 mm thick sheet that illuminated the flow. A PCO Sensicam camera with a resolution of 1280×1024 recorded images of the seeding particles in the laser sheet.

An aqueous dialcohol-glycerol mixture was fed to a Laskin nozzle to create the seeding droplets which had a mean diameter of about 1 μm. To assure a homogeneously seeded measurement area, a large enclosure was built around the set-up. By connecting the inlet of the fan to the enclosure a closed loop was created in which the seeded air was recycled.

For the multiple jet experiments an open wind tunnel was constructed with a square outlet of 30×30 cm^2. An aluminium nozzle plate with 13 nozzles in hexagonal set-up was attached to the wind tunnel outlet. Figure 1 shows a sketch of the flow configuration (a) and the nozzle plate (b). An aluminium nozzle plate with 13 nozzles in hexagonal set-up was attached to the wind tunnel outlet. The diameter of the nozzles was D= 13 mm, the nozzle spacing (or pitch) was s= 26 mm ($2D$) and the thickness of the plate was 2 mm. A glass

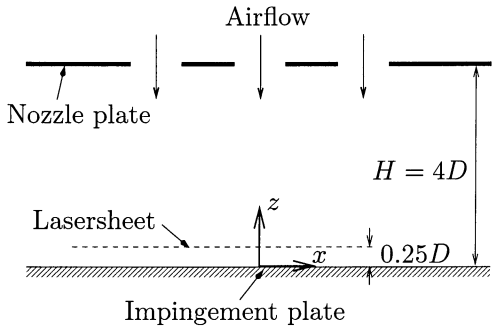

(a) Side view

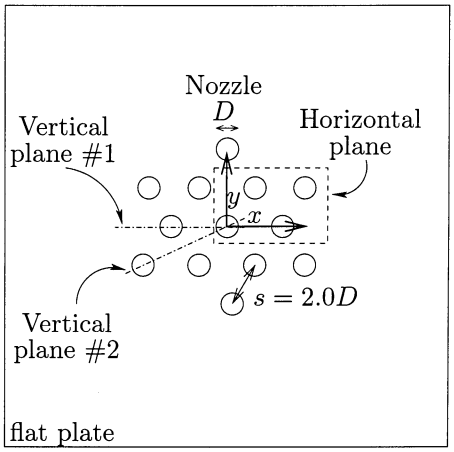

(b) Top view

Figure 1: Flow configuration of multiple impinging jets

impingement plate was placed parallel to the nozzle plate. The distance H between the nozzle plate and the impingement plate was $4D$. The Reynolds number, on the basis of the velocity on the centre line of the central jet and the nozzle diameter, was equal to 18.2 $\times 10^3$.

Measurements were done in one plane parallel to the impingement plate (the horizontal plane) and in two planes parallel to the jets (the vertical planes #1 and #2). For the measurements in the horizontal plane, the camera was placed below the glass impingement plate and a 55 mm lens at a numerical aperture $f^{\#}$ of 8 was used. The size of the measurement area was 53×43 mm^2 ($4.1D\times3.2D$). The plane was positioned at a distance of 3.3 mm ($0.25D$) from the impingement plate, see Fig. 1b. During the measurements the impingement surface was fouled by impacting seeding particles, which blurred the images. This problem was solved by putting a transparency on the glass plate and replacing it when fouled.

The commercial software VidPIV Rowan v4.0 developed by OFS was used to analyse

the images. For the horizontal measurement the velocity vectors were calculated by cross-correlation of 50% overlapping interrogation windows of 64×64 pixels. This yielded vector fields with 1280 vectors with a spatial resolution of 1.3 mm ($0.10D$). The spurious vectors were filtered out and replaced by a linear interpolation procedure. This procedure was repeated twice using an adaptive cross-correlation procedure (with window shifting) to increase accuracy. On average less than 1% of the vectors was spurious.

For the measurements in the vertical planes, the size of the measurement area was 72×52 mm^2 ($5.5D$×$4D$). The camera was equipped with a 105 mm lens at $f^{\#}$=11. In plane #1 the velocities are measured in the central jet and one of its neighbouring jets at a distance of $2D$, while in plane #2 the velocities are measured in the central jet and one of the outer jets at a distance of $2\sqrt{3}D$. Velocity vectors were calculated by cross-correlation of non-overlapping interrogation windows of 32×32 pixels, which yielded 1280 vectors with a spatial resolution of 1.8 mm ($0.14D$). Filtering out and replacing spurious vectors was done analogously to the horizontal measurement. Here also the analysis was repeated twice using an adaptive cross-correlation procedure. The percentage of spurious vectors was less than 3%.

RESULTS AND DISCUSSION

In order to verify our PIV system, we first performed in parallel the PIV and LDA measurements in the single jet set-up. Figures 2a and b present mean and RMS velocity profiles perpendicular to the impingement plate. These profiles resulted from the LDA and PIV measurements in the single jet set-up at a radial distance $r = 0.5d$ from the centreline of the jet. The results presented here were created from an ensemble of 1500 statistically independent snapshots of the flow. Good agreement between the results of both measurement techniques is observed.

In addition, the PIV results in the single jet set-up served for testing various structure identification methods. A preliminary result of this can be found in Figure 3.

Figures 4a and b show the mean velocity and the turbulent kinetic energy k, respectively, in plane #1 in the multiple jet set-up. Figures 5a and b show the same quantities in plane #2. The statistical quantities presented in Figures 4 and 5 were calculated from an ensemble of 3000 statistically independent

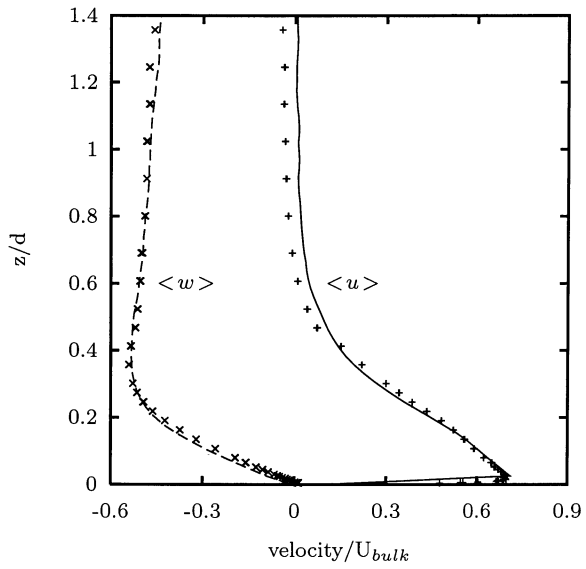

(a) Mean velocities

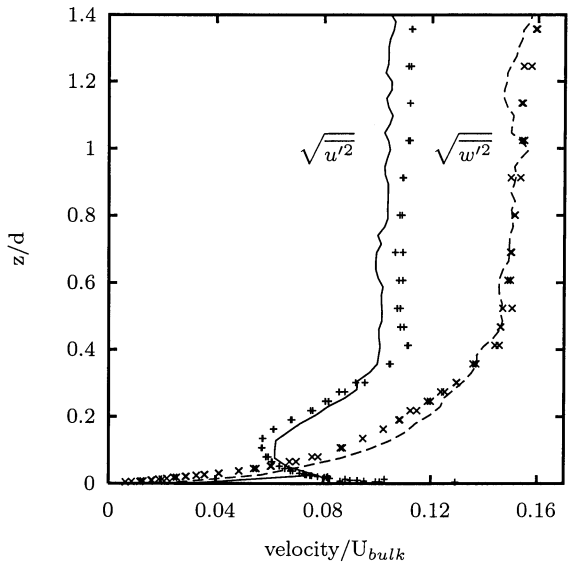

(b) Root mean square velocities

Figure 2: Mean and RMS velocities in a single impinging jet at r/D= 0.5 (LDA= symbols, PIV= lines).

snapshots. The turbulent kinetic energy k was computed from the two component PIV data as $\frac{1}{2}(2\overline{u'^2}+\overline{w'^2})$, assuming that the contribution of the unmeasured third velocity component was $\overline{v'^2} \approx \overline{u'^2}$.

In Figure 4a two counter-rotating recirculation zones are present between the two jets. The air injected through the nozzles impinges on the plate and short wall jets are formed. The wall jets emerging from the impingement points collide and separate from the impinge-

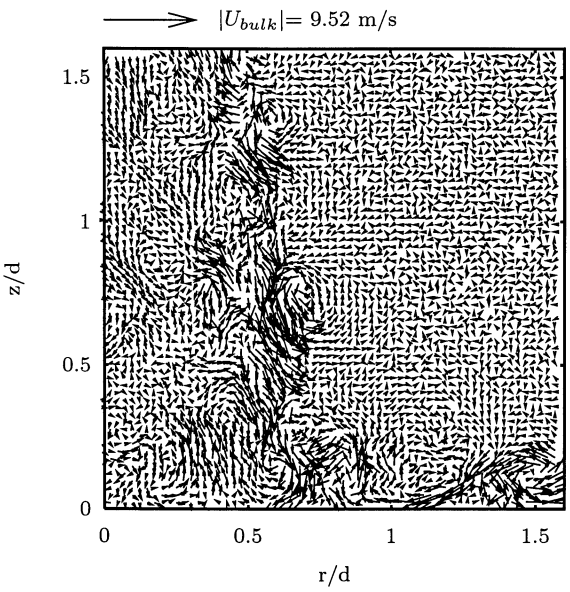

(a) Velocity field

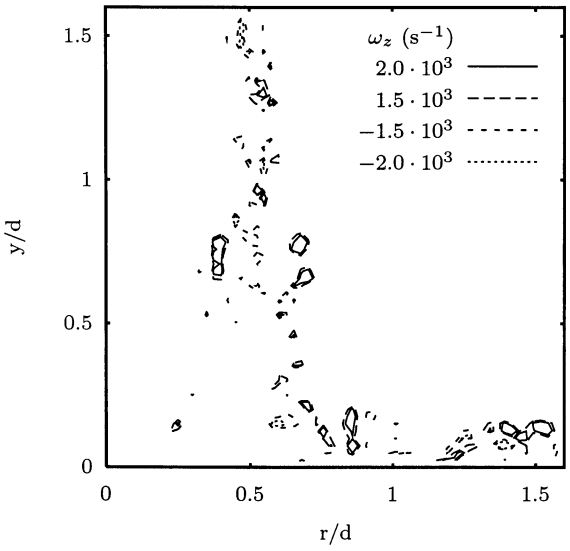

(b) Vorticity field

Figure 3: Fields of instantaneous velocity and vorticity, the ensemble average field was subtracted.

ment plate. Part of the separated air recirculates in the region next to the central jet, while another part is entrained into the neighbouring jets thus forming a discharge mechanism for exhaust air as was reported by Matsumoto et al. (1999). A similar mean flow pattern can be observed for vertical plane #2 in Figure 5. The main difference is the vortical structure with its centre approximately at $(-2.7D, 0.5D)$, which is a horse shoe type vortex that circumscribes the outer most jet.

It is observed from Figures 4b and 5b that the turbulent kinetic energy k is distributed symmetrically about the axis of the centre jet. The edges of the central jet and the inner edge of the neighbouring jets are characterized by regions of high k. However, the outer edge of the neighbouring jets cannot be discerned because k is not concentrated in a narrow region. Furthermore, Figures 4b and 5b suggest that the potential core of the central jet has disappeared within approximately $2.5D$ from the nozzle plate. This was confirmed by a plot of the mean velocity on the axis of the central jet, which showed an essentially constant centreline velocity over a distance of $2D$ after which the centreline velocity steadily decreased towards the impingement plate. Note that the length of the potential core of the central jet ($\approx 2D$) is significantly shorter than the often cited value of $4D$ for the potential core length of a single impinging jet, see e.g. Cornaro et al. (1999).

The mean velocity and the velocity fluctuations in a plane $0.25D$ above the impingement plate are shown in Figures 6a and b, respectively. These fields were created from an ensemble of 1000 statistically independent snapshots. In this case, the contribution to k of the out-of-plane velocity fluctuations $\overline{w'^2}$ is much higher than the contribution of both in-plane velocity fluctuations $\overline{u'^2}$ and $\overline{v'^2}$. For this reason we present values for $\overline{u'^2} + \overline{v'^2}$ in Figure 6b.

Figure 6a shows a nearly hexagonal pattern in the mean flow vector plot with impingement locations almost coinciding with the geometrical centres of the nozzles. Only the outer most jet is slightly displaced which indicates that the crossflow induced by the discharging air is weak.

Figure 6b shows minimum values for the variance of the velocity fluctuations in the impingement regions. Local maxima are found in between the centre jet and its direct neighbours. A region with high variance of the velocity fluctuations is found approximately at $(2.3D, 1.3D)$. This region coincides with the location of the horse shoe type vortex.

A snapshot of the velocity vectors in vertical plane #2 is depicted in Figure 8. At first sight the outer jet is qualitatively not dissimilar to the outer jet the ensemble averaged velocity field shown in Figure 5a. In both the instantaneous and in the ensemble averaged velocity field, the outer jet impinges on the plate while forming a horse shoe type vortex. However, the instantaneous velocity field reveals that at certain time instants the central jet will be ei-

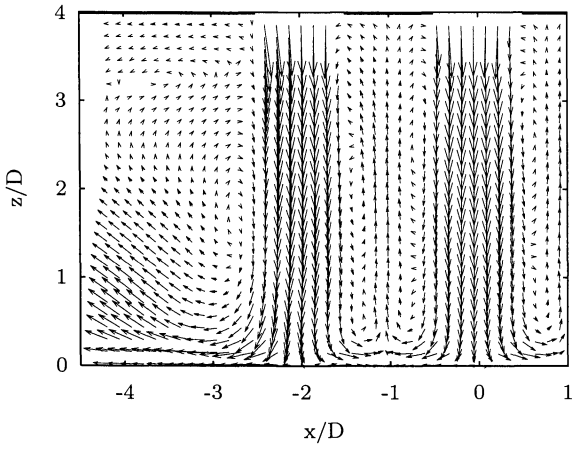

(a) Mean velocity

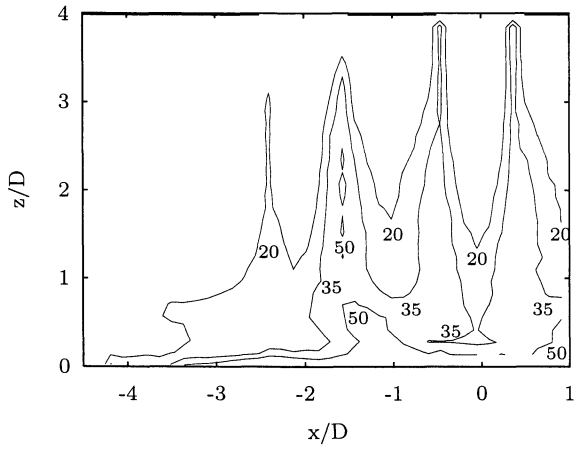

(b) Turbulent kinetic energy k

Figure 4: Statistical quantities in vertical plane #1

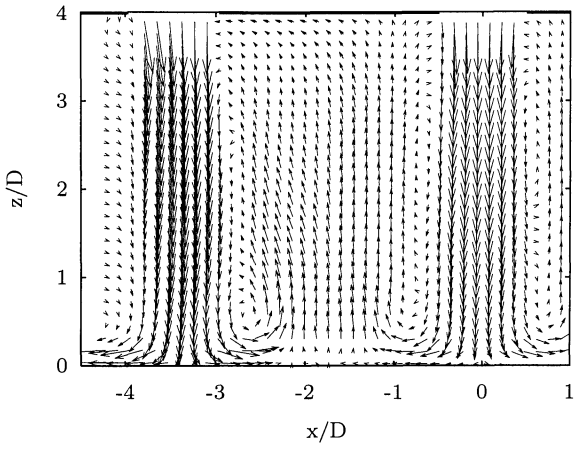

(a) Mean velocity

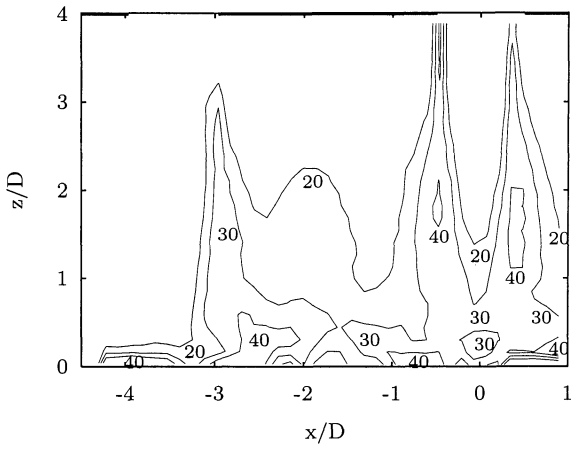

(b) Turbulent kinetic energy k

Figure 5: Statistical quantities in vertical plane #2

ther broken up before impingement takes place or severely displaced out-of-plane. It is not known at this stage whether this large scale phenomenon has a random or quasi-periodic behaviour.

Two snap shots of the velocity field in the horizontal plane are given in Figures 7a and b. The instantaneous velocity field in Fig 7a seems more or less conventional in the sense that it shows the impingement locations in a roughly hexagonal pattern. Slight displacements from the geometrical centres of the nozzles occur due to oscillations in the individual jets. The snapshot depicted in Figure 7b is more interesting because it shows a very strong displacement, or possibly a break up, of the outer most jet. This is in line with the observations made from the instantaneous velocity vectors in the vertical plane.

CONCLUSIONS

First, the consistency of PIV measurements in impinging jets at high Reynolds number was verified. This was done by comparing the results of PIV and LDA measurements at one station in a single impinging jet set-up. Good agreement was observed between the results of both techniques.

Subsequently, results from PIV experiments in a multiple impinging jet set-up were presented. In both the instantaneous and in the ensemble averaged velocity field, a horse shoe type vortex was observed that circumscribes the outer jet of the array. In a plane parallel to the impingement plate at a height of $0.25D$, a region of high turbulent kinetic energy was found which coincides with the location of the horse shoe type vortex. Furthermore, compared to a single impinging jet the potential

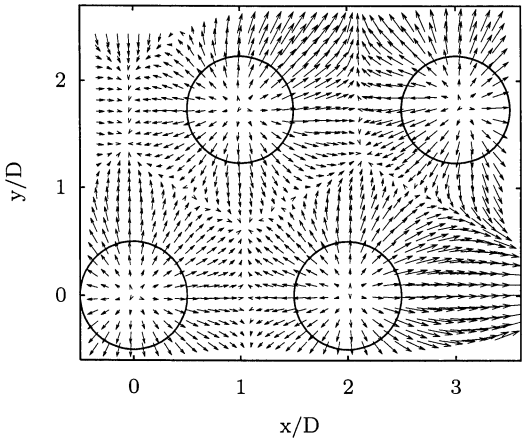

(a) Mean velocity

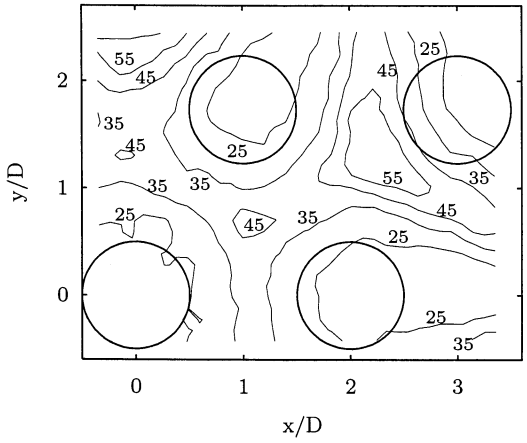

(b) Variance of velocity fluctuations $\overline{u'^2} + \overline{v'^2}$

Figure 6: Statistical quantities in horizontal plane

core of the central jet is significantly shorter.

References

Kataoka, K., 1990, "Impingement Heat Transfer Augmentation due to Large Scale Eddies", *Proceedings of the 9th International Heat Transfer Conference*, G. Hetsroni ed., Hemisphere Publishing Corp., New York, Vol. 1, pp. 255–273.

Cornaro, C., Fleischer, A.S., and Goldstein, R.J., 1999, "Flow Visualization of a Round Jet Impinging on Cylindrical Surfaces", *Experimental Thermal and Fluid Science*, Vol. 20, pp. 66–78.

Martin, H., 1977, "Heat and Mass Transfer between Impinging Gas Jets and Solid Surfaces", *Advances in Heat Transfer*, Academic Press, Vol. 13, pp. 1–60.

Moustafa, G. H., and Rathakrishnan, E., 1993, "Studies on the Flow Field of Multijet with Square Configuration", *AIAA Journal*, Vol. 31, No. 7, pp. 1189–1190.

Matsumoto, R., Ishihara, I., Yabe, T., Ikeda, K., Kikkawa, S., and Senda, M., 1999, "Impingement Heat Transfer within Arrays of Circular Jets Including the Effect of Crossflow", *Proceedings of the 5th ASME/JSME Joint Thermal Engineering Conference*, California, no. AJTE99-6386.

Viskanta, R., 1993, "Heat Transfer to Impinging Isothermal Gas and Flame Jets", *Experimental Thermal and Fluid Science*, Vol. 6, pp. 111–134.

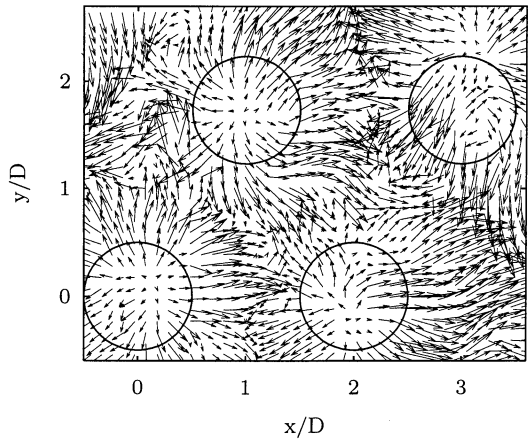

(a) Horizontal plane, shot 1

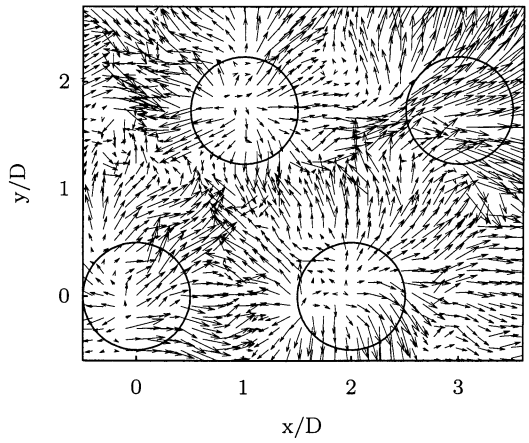

(b) Horizontal plane, shot 2

Figure 7: Two snapshots of the flow in the horizontal plane

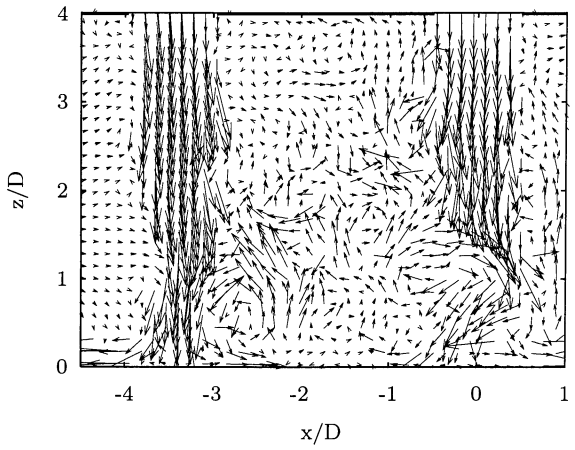

Figure 8: Snapshot of the flow in vertical plane #2